PLANT SCIENCES

Twilight length alters growth and flowering time in Arabidopsis via *LHY/CCA1*

Devang Mehta[1,2,3], Sabine Scandola[3], Curtis Kennedy[4], Christina Lummer[3], Maria Camila Rodriguez Gallo[3], Lauren E. Grubb[3], Maryalle Tan[3], Enrico Scarpella[3], R. Glen Uhrig[3,5]*

Decades of research have uncovered how plants respond to two environmental variables that change across latitudes and over seasons: photoperiod and temperature. However, a third such variable, twilight length, has so far gone unstudied. Here, using controlled growth setups, we show that the duration of twilight affects growth and flowering time via the *LHY/CCA1* clock genes in the model plant Arabidopsis. Using a series of progressively truncated no-twilight photoperiods, we also found that plants are more sensitive to twilight length compared to equivalent changes in solely photoperiods. Transcriptome and proteome analyses showed that twilight length affects reactive oxygen species metabolism, photosynthesis, and carbon metabolism. Genetic analyses suggested a twilight sensing pathway from the photoreceptors *PHY E*, *PHY B*, *PHY D*, and *CRY2* through *LHY/CCA1* to flowering modulation through the *GI-FT* pathway. Overall, our findings call for more nuanced models of day-length perception in plants and posit that twilight is an important determinant of plant growth and development.

INTRODUCTION

The circadian clock is a molecular network that generates an approximate 24-hour oscillatory period that responds to acute changes in various environmental cues such as light and temperature to regulate the diel cycling of physiological activity in all eukaryotes. The plant circadian clock is especially complex, composed of multiple, interconnected transcription-translation feed-forward loops that are reset by the onset of dawn and buffered against mild changes in temperature (*1*). The clock itself has a far-reaching regulatory capacity, directly and indirectly controlling nearly all physiological processes from photosynthesis, energy metabolism, and even biotic stress response (*2*).

Over the lifecycle of a plant, changes in photoperiod and temperature coincide with circadian rhythms to induce developmental changes such as the transition to flowering. These changes are governed by seasonality, which varies depending on the latitude at which a plant is grown. Changes in latitude determine seasonal temperature, photoperiod, as well as the length of dawn and dusk (i.e., twilight length) (*3*). The effect of seasonal changes in temperature and photoperiod on both the circadian clock and flowering has been well studied in a range of plant species. For example, mutations in clock genes such as *ELF3* and *PRR7* orthologs have been linked to the successful migration of bean and alfalfa from tropical to temperate latitudes (and consequently, to the associated changes in temperature and photoperiod) (*4*–*6*). More recently, a simple translational coincidence model has emerged suggesting that overlap between clock-controlled transcript phases and light-dependent protein synthesis explains molecular adaptation to new photoperiods due to changing seasons (*7*).

Foundational work on the plant circadian clock has been conducted using rectangular light-dark (LD) cycles with multispectral high-intensity sodium or fluorescent tube lights that are turned on or off in a defined period. [However recently, light-emitting diode (LED) lights have been used in luciferase assays of clock function (*8*).] Over the past two decades, this general setup has led to groundbreaking discoveries in plant chronobiology, from the discovery of the clock components themselves to global transcriptional profiling and modeling under different diel light regimes (*7*, *9*–*13*). However, the use of these light setups along with a rectangular LD cycle is a poor match to real-world conditions, particularly at temperate and polar latitudes where relatively long twilights and lower peak light intensities are present. Thus, largely due to technical limitations in laboratory and greenhouse lighting systems, the impact of changing durations of twilight, i.e., the gradual change in light intensity between night and day, remains unstudied in plants.

Given ongoing climate change and the global rise in temperatures (*14*), it is expected that crop varieties and crop species adapted for warmer, southern latitudes will gradually be adopted in temperate zones that feature different seasonal photoperiod changes and twilight length (*15*). This phenomenon of northward migration has already been found to occur over the past 40 years in rain-fed wheat, maize, and rice (*16*). Latitudinal migration is also expected to play a role in future agriculture through the expansion of the agricultural climate zone northward due to global warming (*17*). It is thus crucial to develop a fundamental understanding of how variation in the latitudinal light environment, including changes in twilight length, affects plant growth and development.

Here, we present results from experiments examining the impacts of varying lengths of twilight on the model plant Arabidopsis using multispectral LED lights with precise intensity control. To simulate different twilight regimes in the laboratory, we must make approximations, focusing on twilight as defined as the period of gradual change in light intensity before sunrise and after sunset. We rely on the definitions listed by the United States Navy's Astronomical Information Center (https://aa.usno.navy.mil/faq/RST_defs) and use durations of civil twilight measurements at different latitudes to simulate different lengths of light intensity ramps in our laboratory conditions. While our setup is not an exact reflection of

[1]Department of Biosystems, KU Leuven, B-3001 Leuven, Belgium. [2]Leuven Plant Institute, KU Leuven, B-3001 Leuven, Belgium. [3]Department of Biological Sciences, University of Alberta, Edmonton, AB T6G 2E9, Canada. [4]Department of Computing Science, University of Alberta, Edmonton, AB T6G 2E9, Canada. [5]Department of Biochemistry, University of Alberta, Edmonton, AB T6G 2E9, Canada.
*Corresponding author. Email: ruhrig@ualberta.ca

natural light, it permits us to study the impact of light intensity ramps similar to natural twilight while controlling for factors such as daily light integral (DLI). In this respect, our conditions are more reflective of natural light than other circadian-controlled growth environment experiments conducted in plant systems to date.

Our results demonstrate that twilight length affects plant vegetative growth and flowering time differently. We also show that twilight measurement requires the morning components of the plant circadian clock. We further present transcriptomic and proteomic data highlighting twilight length–dependent protein-level regulation in select biological pathways. Collectively, our results point to the need for revisiting established ideas regarding core circadian clock functions like photoperiodism by using more natural environmental transitions than previously used in the field.

RESULTS AND DISCUSSION

To investigate the effects of twilight length on plant growth and development, we devised an experimental setup that uses a six-band LED light fixture with fully programmable spectra and sigmoidal ramping of light intensity in controlled growth chambers. We used this setup to gain a comprehensive understanding of the impact of changing twilight lengths on *Arabidopsis thaliana* (Col-0) plants at both physiological and molecular levels, studying the effect of a wide range of twilight lengths (0, 15, 30, 60, and 90 min) on plant growth. These conditions approximate summer twilight lengths at the Equator (~15 min) up to 59°N (~90 min) (https://aa.usno.navy.mil/faq/RST_defs), while the 0-min condition is typical for most plant biology experimentation in controlled growth environments and serves as our no-twilight control. Our experiment was designed to isolate the impact of twilight duration on plant growth, separate from other twilight-associated phenomena such as changes in total DLI (daily light integral; the number of photosynthetically active photons delivered over a 24-hour period) and altered wavelength distribution that might affect photosynthetic capacity. Hence, our LD curves ensured that while the length of the dawn/dusk ramp varied, the DLI remained the same between conditions, with relatively minor changes in peak light intensity [<14 μmol m^{-2} s^{-1} difference in peak photosynthetic photon flux density (PPFD) between the various light regimes] (Fig. 1A and table S1). We also did not alter the light spectrum over the day as this study focused on the impact of light intensity changes over time, rather than an accurate simulation of natural twilight. However, our light spectrum included a supplemental far-red light component (red:far-red ratio ~ 1), which according to the recent discoveries by the Imaizumi laboratory is important for mimicking flowering under natural conditions (*18*, *19*).

We first analyzed plant growth by measuring plant area (total area of the rosette) using overhead RGB cameras and processing images using the open-source PlantCV image analysis software (*20*, *21*). Measurements of plant area from images acquired 25 days after imbibition showed that *A. thaliana* Col-0 (Arabidopsis) plants grew to larger sizes as twilight length increased to an optimum of 30 and 60 min, with a median increase in plant area of 34% compared to plants grown under a no-twilight rectangular LD cycle (table S2). Plants grown under the extended 90-min twilight condition, however, showed no increase in plant size relative to the no-twilight condition (Fig. 1B). This trajectory of plant size increasing with longer durations of twilight up to an optimum of 30 to 60 min was mirrored by plant biomass (fresh weight) measurements taken at 25 days after imbibition. We found that increasing the length of twilight led to a median 16% increase in biomass with a 60-min twilight duration, but no significant change in biomass upon growth with a 90-min twilight compared to the no-twilight control (Fig. 1C and table S3).

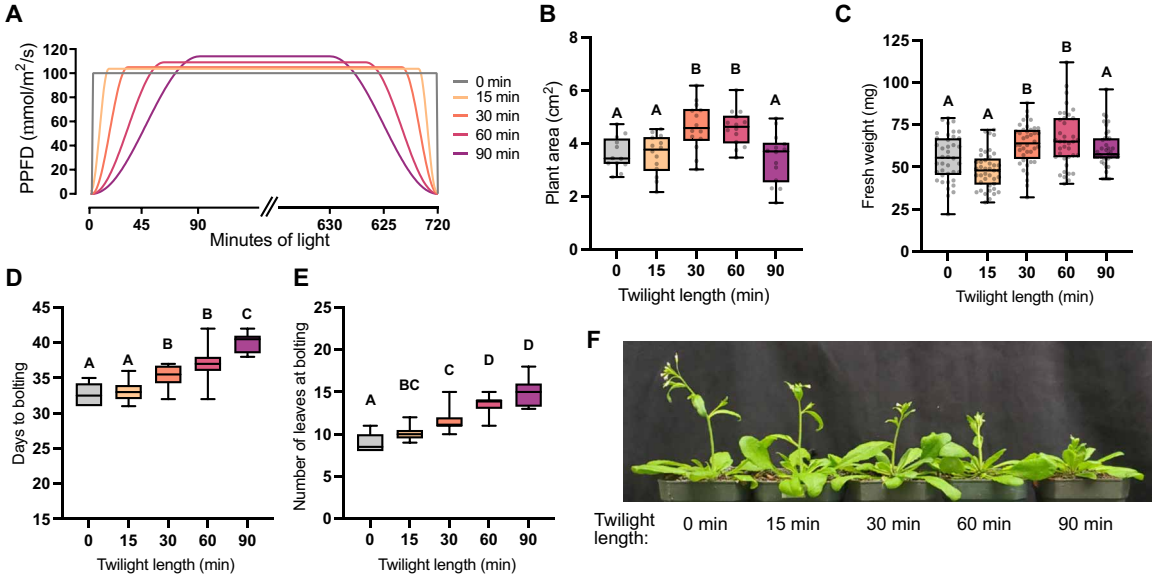

Fig. 1. The impact of twilight length on plant growth and development. (**A**) Twilight length experimental schemes. (**B**) Leaf area of WT plants as measured using PlantCV from rosette images at 25 days after imbibition ($n > 12$). (**C**) Fresh weight of plants grown under different lengths of twilight ($n > 38$ plants) measured at 25 days after imbibition. (**D** and **E**) Flowering time measured by counting the number of days to bolting and the number of leaves at bolting respectively ($n > 10$ plants). (**F**) Representative images of plants at 36 days after imbibition. Letters above all graphs depict significantly different data points based on a one-way ANOVA and Tukey's post hoc test with adjusted $P < 0.05$.

These results were validated in an independent replication of the experiment (fig. S1).

Next, we assessed how this twilight-induced increase in plant size affected plant development by measuring flowering time in wild-type (WT) Arabidopsis plants. Time to flowering or time to bolting can be measured using either direct time measurements (days to bolting) or morphometric indicators such as the number of rosette leaves at bolting (*22*). In our twilight length experiment, both days to bolting and the number of rosette leaves at bolting increased linearly with twilight length, including in the 90-min extended twilight condition (Fig. 1, D and E, and table S4). This result was replicated in an independent experiment (fig. S1). The fact that an extended period of twilight (90 min) does not result in any increase in vegetative growth (as measured by plant area and biomass) but lengthens flowering time is intriguing as vegetative growth and flowering time are highly correlated in a variety of phenological studies, under different altitudes, latitudes, and genotypes (*23*–*25*). The relationship between vegetative growth and flowering time is regarded as a classic example of a life-history trade-off with strong genetic underpinnings (*26*). In *A. thaliana*, previous studies using different photoperiodic regimes have noted a difference in the relationship of flowering time as measured in days to bolting versus leaf count at bolting with decreasing photoperiods. For example, below the so-called "ceiling photoperiod" of ~8 hours, flowering time measured in days continues to increase linearly, while leaf number at bolting remains constant (*27*). Thus, our finding that a 90-min period of twilight breaks the relationship between vegetative growth and flowering time calls for a re-evaluation of our understanding of the limits of the growth-reproduction trade-off in plants, particularly at very high latitudes. Furthermore, the fact that this disconnect occurs below the previously defined "ceiling photoperiod" suggests differences between how plants sense photoperiod (or more precisely, how they sense the duration of photosynthetically active radiation) and their means of sensing twilight duration. Recent targeted research has begun to unravel how photosynthetic day length is timed differently from "absolute photoperiod" in Arabidopsis under standard experimental LD conditions (*28*).

To further examine the differences between responses to twilight length and photoperiod, we next performed a second experiment where plants were grown under a series of decreasing photoperiods with a rectangular LD scheme and compared to a 30-min twilight as a control. The photoperiod series was designed to test: (1) how sensitive plants are to minute changes in photoperiod and (ii) whether a minimum amount of light intensity is necessary to result in the plant growth and developmental changes seen under twilight conditions. This second question was guided by previous studies which established that while most plant photoreceptor signaling is saturated at <5 μmol m^{-2} s^{-1}, net carbon fixation only occurs beyond 8 to 40 μmol m^{-2} s^{-1} (*29*, *30*). The results described in Fig. 1 suggest the hypothesis that as light intensity ramps up and down during twilight, different processes turn on and off at different times, potentially resulting in differential regulation of vegetative growth and flowering time. Hence, under more natural conditions, the concept of "photoperiod sensitivity" might encompass two temporally separated phenomena where (i) plants sense the onset of day and night at very low light intensities (this might also be when the clock is "reset") and (ii) metabolic processes more directly tied to growth (e.g., carbon fixation) commence and end at higher light intensity thresholds (potentially in concert with the clock). Prior research into photoperiod sensitivity may not have been able to separate these processes due to the use of rectangular LD cycles.

By contrast, the experimental scheme described in Fig. 2A permitted us to test the sensitivity of flowering time to 4-, 10-, 30-, and 60-min reductions in photoperiod. Furthermore, by including a 30-min twilight condition, this experimental design also allowed us to test a light intensity range of 2.6, 7.07, and 41.64 μmol m^{-2} s^{-1} as light detection thresholds that most closely explain the phenotype under a 30-min twilight condition (light intensity intercepts of the 30-min ramp and successive rectangular photoperiod LD schemes; see Fig. 2A). For instance, if the 5sq condition (a 10-min photoperiod reduction) most closely phenocopied the 30-min twilight treatment, we might conclude that a photoperiodic-light detection threshold close to 7.07 μmol m^{-2} s^{-1} was in effect under this twilight condition. However, our results show that only a 30-min reduction in photoperiod (15sq) comes close to the 30-min twilight treatment in terms of a delay in flowering time (Fig. 2, B and C, and table S6). This implies that if we use a model where plants purely measure photoperiod (i.e., only the *x* axis in Fig. 2A) rather than the slope of

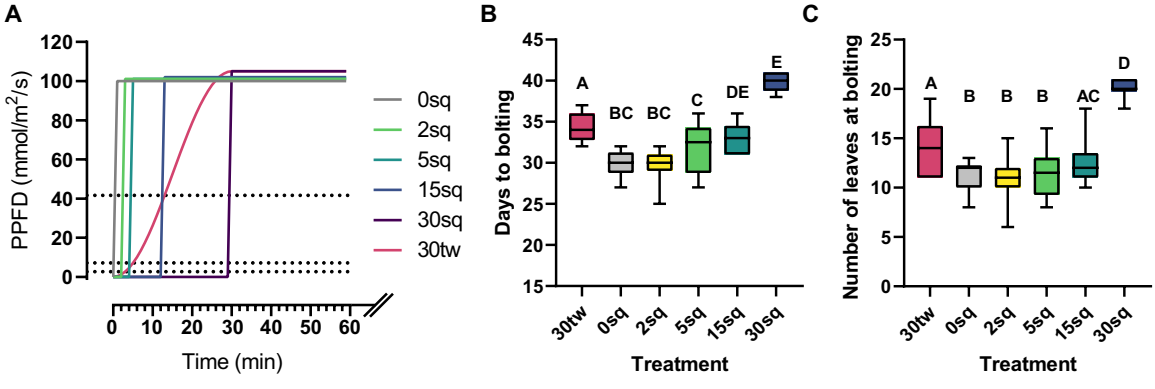

Fig. 2. Dissecting the differences between plant responses to twilight and photoperiod. (**A**) Depiction of the light treatments in this experiment from a 12-hour light:12-hour dark photoperiod (0sq) to 2- (2sq), 5- (5sq), 15- (15sq), and 30-min (30sq) reductions in photoperiod in the morning and evening (only morning shown). A 30-min twilight condition (30tw) is included as control. Dotted lines depict light intensity at different points along the twilight ramp. Flowering time measurements in terms of (**B**) days to bolting and (**C**) number of leaves at bolting of WT plants grown under the conditions depicted in (A). A minimum of 12 plants per treatment were measured. Letters depict significantly different data points based on a one-way ANOVA and Tukey's post hoc test with adjusted $P < 0.05$.

light intensity at the start and end of day, this measurement must begin and end past ~40 µmol m^{-2} s^{-1} of light intensity during the ramp to explain the flowering phenotype observed. However, the increase in flowering time over successive reductions in photoperiod is also nonlinear, in contrast to the twilight length experiment shown in Fig. 1 (D and E). In addition, a light detection threshold of ~40 µmol m^{-2} s^{-1} is far higher than previously measured thresholds for photoreceptor activation. Collectively, this shows that twilight length affects flowering time and that this effect can only partially be explained by differential photoperiod sensing under different twilight length regimes. It is thus imperative that future research into clock function and seasonal sensitivity use more sophisticated experimental designs to account for the differential regulation of growth and flowering under more natural LD transitions.

Since flowering time and seasonal sensitivity are intimately tied to circadian clock function and because we observed twilight length–associated changes in clock period, we next studied the flowering response of a suite of core clock mutants to different lengths of twilight. We found that both clock activator mutants (*rve 4 6 8*) and two clock repressor mutants (*toc1-2* and *elf4-101*) showed more similar flowering time changes to WT plants, with progressive increases in twilight length (fig. S2). However, the double mutant of the morning element of the clock, *lhy cca1* showed a near-complete insensitivity to changes in twilight length, with significant changes in flowering time observed only under the 90-min twilight treatment (Fig. 3 and table S4). To see if this absence of twilight sensitivity also manifested in growth outcomes, we monitored plant area and biomass for *lhy cca1* plants, finding smaller changes in plant area (Fig. 3A) and biomass (Fig. 3B) at different twilight lengths compared to WT plants (Fig. 1, A and B). These results were replicated in an independent experiment (fig. S1). Together, our results suggest that the LHY/CCA1 module of the clock is key to sensing not only effective photoperiod but also the duration of twilight, i.e., the slope of increasing and decreasing light intensity.

To identify the pathway from twilight length perception to the clock, we performed a screen of characterized homozygous photoreceptor knockout mutants under the 0-, 30-, and 90-min twilight length conditions. Here, we found that *phye* and, to a lesser extent, *phyd* closely phenocopy the twilight-insensitive flowering response of *lhy cca1*. We also confirmed that the twilight-insensitive flowering response of *lhy cca1* is phenocopied by *phyB* and *cry2* (fig. S3). Previous research has found connections between *PHYA*, *PHYB*, and *CRY2* and photoperiodic flowering (*31*–*34*), as well as direct connections to the circadian clock through *LHY/CCA1* (*31*, *35*–*39*). However, we were not able to find any involvement of *PHY A* in twilight length perception.

Next, we sought to determine which of the flowering pathways was responsible for the twilight sensing phenotype. Hence, we examined flowering time mutants *gi-200*, *ft-10*, *soc1-2*, and *flc-1* under different twilight conditions. *GI* is a key player in the photoperiodic flowering pathway (*12*, *40*, *41*), while *FLC* is a flowering regulator in autonomous flowering (*42*). *FT* encodes for the primary florigen signal to control flowering time (*43*), while *SOC1* is positively regulated by *FT* and negatively regulated by *FLC* to modulate flowering (*44*). Here, we found that *gi-200* and *ft-10* are unresponsive to twilight, phenocopying *lhy cca1*, while *soc1-2* and *flc-1* remain twilight responsive similar to WT plants (fig. S4). Collectively, these data suggest that our twilight length–dependent flowering phenotypes manifest via a *GI-FT* signaling mechanism and not via an *FLC-SOC1* photoperiod-independent pathway.

To view the molecular impacts of increasing twilight duration in plants, we next performed a comparative quantitative proteomic and transcriptomic analysis of WT and *lhy cca1* plants. Plants grown under the same light conditions described above were sampled 25 days after imbibition, at ZT23, approaching the time of peak LHY/CCA1 expression. Proteomic analysis was carried out using our newly developed label-free BoxCarDIA quantitative proteomics methodology for more consistent protein quantification across the different twilight treatments (*45*). Transcriptomic analysis was performed using a modified Smart-seq2 protocol for cost-effective bulk RNA sequencing (RNA-seq) (*46*). This allowed us to quantify a total of 5748 protein groups and 21,126 transcripts, of which 4746 protein groups and 11,728 transcripts were quantified across all the samples and replicates (tables 6 and 7). For both the protein and transcript datasets, we performed two differential analyses: (i) comparing WT and *lhy cca1* plants at each twilight length (Fig. 4, A and B, and table S8) and (ii) comparing each twilight length to the no twilight treatment for each genotype (Fig. 4, C and D, and table S9). The former showed that the number of differentially abundant proteins in *lhy cca1* plants compared to WT increased under longer twilights. By contrast, the number of differentially expressed genes in *lhy cca1* plants peaked in the 30-min twilight treatment and was the lowest under 90 min of twilight. This pattern of transcriptional change appears to mirror phenotypic differences between *lhy cca1* and WT plants under different

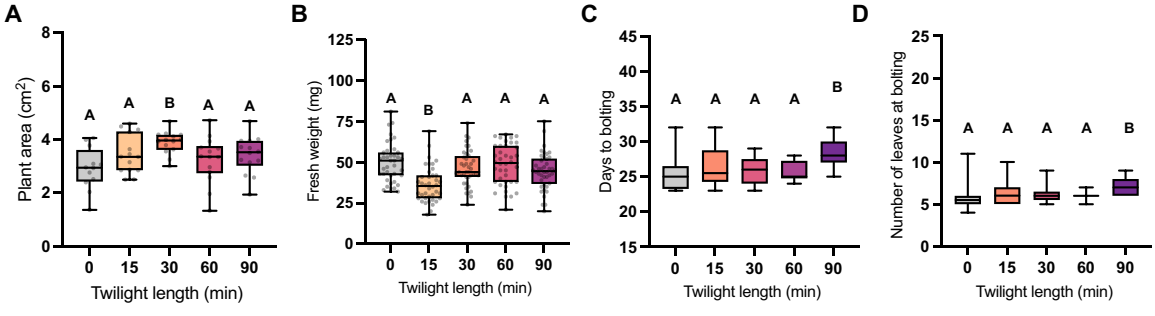

Fig. 3. *lhy cca1* plants exhibit a muted phenotypic response to different twilight lengths. (**A**) Leaf area of *lhy cca1* plants at 25 days after imbibition measured using PlantCV ($n > 12$). (**B**) Fresh weight measurements of *lhy cca1* plants at 25 days after imbibition ($n > 39$). (**C** and **D**) Flowering time measured in terms of (C) the number of leaves at bolting and (D) days to bolting ($n > 22$). Letters depict significantly different data points based on a one-way ANOVA and Tukey's post hoc test with adjusted $P < 0.05$.

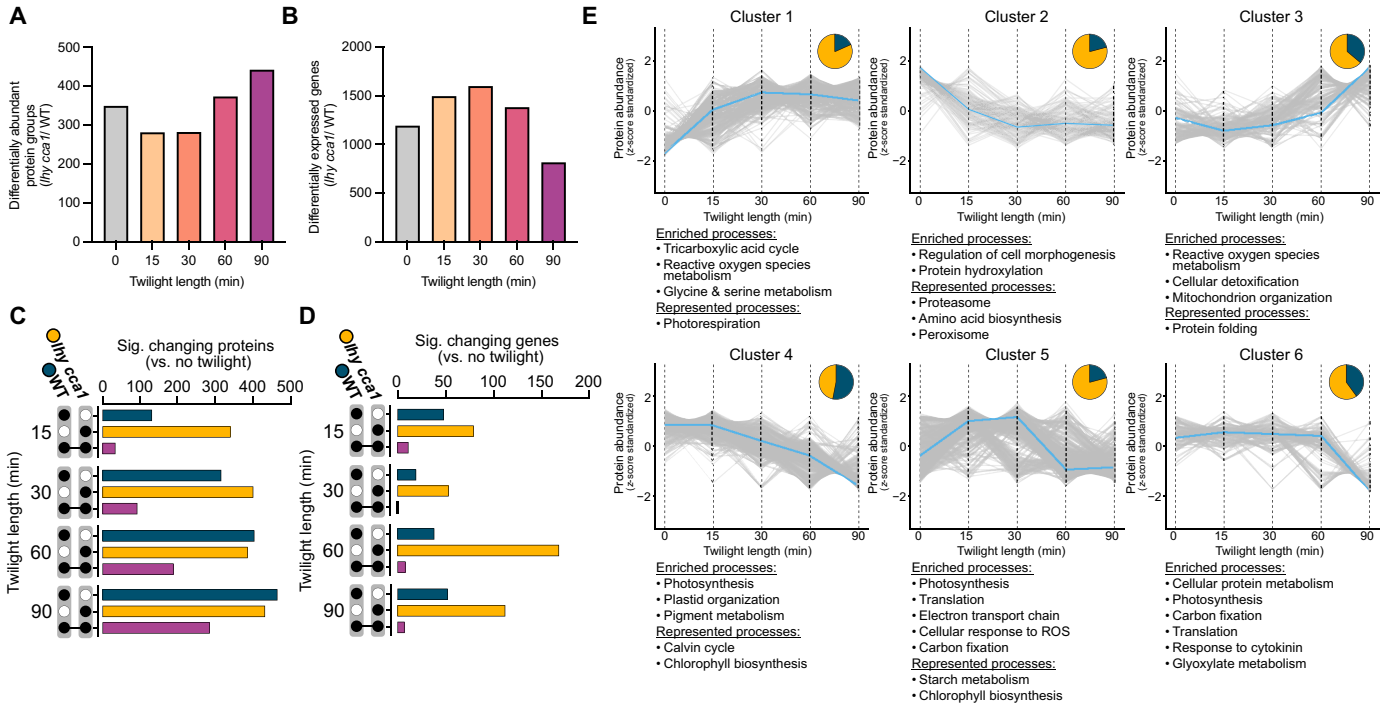

Fig. 4. Proteome and transcriptome dynamics under different periods of twilight. (**A**) Number of proteins that change significantly in abundance at each of the different twilight durations in *lhy cca1* compared to WT plants. (**B**) Number of differentially expressed genes between *lhy cca1* and WT plants at each twilight length. (**C**) Upset plot showing the overlaps in proteins significantly changing in abundance and (**D**) differentially expressed genes under different twilight durations (compared to no twilight) in both *lhy cca1* and WT plants. (**E**) Shape-based clustering of protein abundance (*z*-score standardized) with clusters annotated with enriched Gene Ontology terms and selected member proteins and pathways. Blue lines show cluster centroids. Pie charts show the proportion of proteins in each cluster found in *lhy cca1* (yellow) and WT (blue) samples. ROS, reactive oxygen species.

twilights, with both the transcriptome and phenotype of *lhy cca1* approaching that of WT plants under the extended twilight. We next focused on analyzing proteins and transcripts changing across each twilight treatment compared to the no twilight condition for each genotype. Here, we identified much greater twilight-dependent protein-level regulation compared to transcriptome alteration in both genotypes. The number of differentially abundant proteins at each twilight treatment (compared to no twilight) increased linearly with twilight length for both genotypes (Fig. 4C) from 173 proteins in WT and 381 in *lhy cca1* under 15 min of twilight to as many as 755 in WT and 722 in *lhy cca1* under the 90-min twilight treatment. [Note that the upset plots in Fig. 4C separate these numbers to depict the number of differentially abundant proteins exclusive to each genotype and in common to both (in purple)]. The number of differentially abundant proteins in common between the two genotypes also increased under longer twilights. In stark contrast, we found very few differentially expressed genes in both genotypes (but especially WT plants), with a maximum of 63 genes differentially expressed in WT plants grown under 15 min of twilight (versus no twilight) and 180 differentially expressed genes in *lhy cca1* plants grown under 60 min of twilight (versus no twilight) (Fig. 4D). Given that proteomics typically involves measurements of far fewer gene products than RNA-seq analysis, it was unexpected to find a greater number of differentially abundant proteins than differentially expressed genes. Hence, we believe that the twilight response likely involves greater protein-level regulation (such as differential protein synthesis or degradation) than transcriptional regulation.

To identify biological processes potentially subject to such protein-level regulation, we next clustered proteins quantified across all replicates and treatments in our analysis by the shape of their *z*-score standardized abundance over different twilight lengths. Clustering analysis was performed on the subset of proteins that changed significantly in their abundance dependent on twilight length [analysis of variance (ANOVA) $P < 0.05$] in each genotype. We partitioned the data into six clusters depending on the shape of their abundance trajectories, thereby clustering proteins whose abundance changed similarly over different twilight lengths (Fig. 4E). We then performed Gene Ontology enrichment analysis for each protein cluster as well as StringDB analysis (*47*) to identify both enriched biological processes as well as other pathways represented by the constituent proteins in each cluster. Here, we found that clusters 1, 2, and 5 were dominated by proteins changing in abundance in *lhy cca1* plants, while clusters 3, 4, and 6 contained a higher number of proteins changing in abundance in WT plants. Overall, proteins in clusters 1, 3, and 5 followed trajectories that either paralleled or antiparalleled the growth phenotypes observed, either peaking or reaching their lowest abundance under 30 to 60 min of twilight. The two clusters that contained proteins increasing in abundance over longer twilights (1 and 3) were enriched in proteins relating to reactive oxygen species metabolism, glycine and serine metabolism, and cellular detoxification. Cluster 1 also contained proteins involved in photorespiration (which intersects with glycine and serine metabolism). This suggests the hypothesis that optimal lengths of twilight might allow plants to more appropriately manage photooxidative stress. We also

found proteins involved in proteasome and amino acid biosynthesis to be enriched in cluster 2 and proteins involved in cellular protein metabolism enriched in cluster 6, perhaps explaining the difference between the number of differentially abundant proteins and transcripts observed in Fig. 4 (C and D). Last, we also found proteins involved in photosynthesis, both in light harvesting and carbon fixation, to be enriched in clusters 4, 5, and 6. Overall our omics results highlight wide-ranging proteome-level changes associated with longer twilight lengths, specifically implicating the management of oxidative stress and photosynthesis in conjunction with proteasome and translational regulation in the observed twilight-responsive phenotypic changes in WT and *lhy cca1* plants.

A central question in circadian biology is: "How do plants measure the length of day and night across changing seasons?" The use of rectangular LD cycles to perform photoperiod experiments in the past has implied a simplified go/no-go process whereby plants measure day length simply by timing the number of hours between the instantaneous onset of light from 1 day to the next. This view would suggest that plants perceive day and night as a digital "on-off" signal rather than the gradual transition it is in real life. By comparing rectangular LD photoperiods and a series of more natural twilight ramps, we show that plant photoperiod sensing (via the LHY/CCA1 clock genes) affects development not only by measuring the total number of hours or minutes of light but also via more subtle tuning by the amount of light incident over a time interval at day-night transitions (i.e., the slope of light intensity over time). Another alternative hypothesis for day length perception remains that plants might perceive gradual changes in light intensity in the mornings and evenings but nevertheless convert this analog signal to a binary output when triggering photoperiodic flowering, by imposing a high irradiance threshold, similar to that recently found for morning *FT* induction via *PHYA* (*19*). Our findings do not entirely contradict this idea, but the results depicted in Fig. 2 impose a threshold of at least 40 μmol m^{-2} s^{-1} for such a high-irradiance threshold model. Furthermore, our study of phytochrome mutants does not implicate *PhyA* in twilight length sensing. Our follow-up genetic analyses (along with the published literature) allow us to postulate a linear genetic pathway from *PHYE*, in conjunction with *PHYB*, *PHYE,* and *CRY2*, to *LHY/CCA1* to *GI* and *FT* as being responsible for the twilight length-dependent flowering phenotype we observed (Fig. 5). It should be noted that while, in our opinion, the most parsimonious explanation for our findings is that *LHY/CCA1*-mediated twilight length perception occurs via the circadian clock, it is also possible that a clock-independent pathway via direct control of *FT* by *CCA1* (*10*) is responsible.

Future work will aim to study this proposed pathway in greater depth and delineate the roles of these genes in twilight versus laboratory-based rectangular photoperiod sensing. Furthermore, our combined transcriptomic and proteomic analysis leads us to hypothesize that the growth and developmental phenotypes affected by changing twilight lengths are the result of systemic proteome-level regulation (via a regulatory proteasomal-translational control axis) of reactive oxygen species metabolism, photosynthesis, and carbon metabolism. Future targeted studies may resolve exactly how clock control of twilight perception alters these processes to optimize growth during natural photoperiod transitions.

Collectively, we believe that our results offer a more refined understanding of how the circadian clock interprets day length changes in natural environments. It should be noted that our experimental design focused exclusively on studying the impact of twilight length

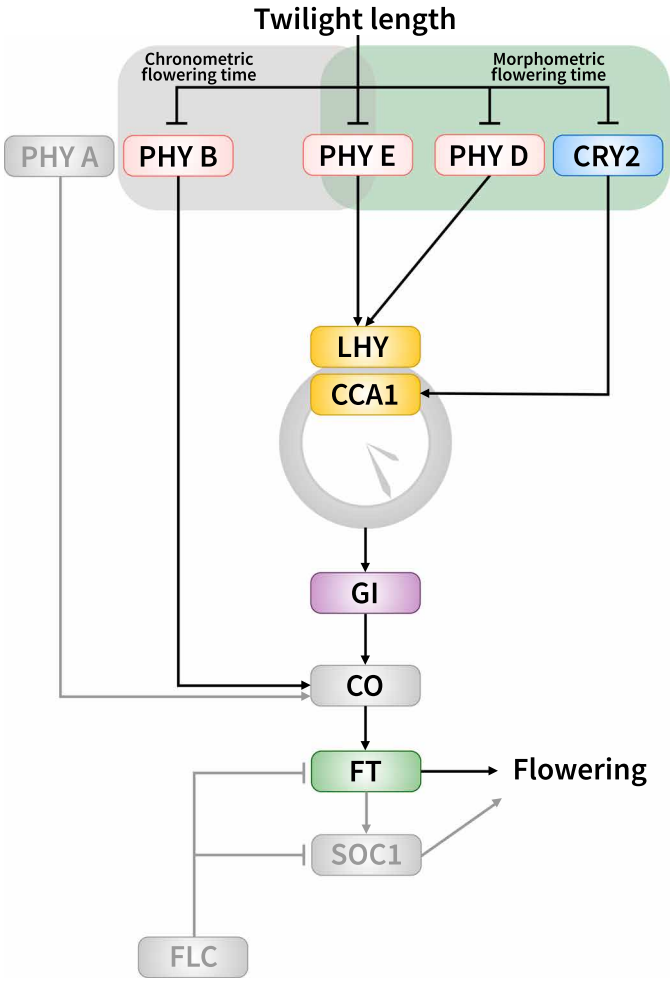

Fig. 5. Proposed genetic pathway connecting twilight length to flowering time. Genes depicted in color are genetically linked to twilight length sensing (via chronometric or morphometric flowering time changes, or both) according to this study, while grayed-out genes are not.

by controlling the DLI between treatments. Natural twilight length variation is of course not independent of changes in DLI and includes changes in spectral composition over the course of a day. Future work in this domain could iterate our experimental design to factor in more realistic twilight and spectral changes, including at different latitudes, different altitudes, and the impact of changes in cloud cover or pollution among other geographical influences on plant growth and development. Furthermore, given the molecular complexity and agronomic value of the traits measured in this study (i.e., growth and flowering time), we expect that our systems-level molecular results to inform future targeted work focused on identifying genes and pathways influencing photoperiodic flowering and diel plant growth modulation over natural light transitions, leading to new breeding and engineering targets. In conclusion, our results add to a growing focus on understanding plant chronobiology from a biogeographical point of view (*48*) and demonstrate that simulating more natural environmental changes can lead to a more nuanced understanding of well-studied clock-controlled processes, such as photoperiodism.

METHODS

Growth cabinet design and construction

Growth cabinets with ventilation holes were constructed using black acrylic and housed in Conviron walk-in growth chambers. The inner walls of the cabinets were lined with reflective Mylar material to ensure uniform lighting. Light bars were equipped with six different LEDs (G2V Optics Inc., Alberta, Canada) with wavelengths (table S1) programmed to approximate the AM1.5 reference spectrum.

Plant growth

A. thaliana (Col-0), *lhy-20 cca1-1* [*lhy cca1*; (*49*)], *rve 4-1 6-1 8-1* [*rve 4 6 8*; (*50*)], *elf4-101* (*51*, *52*), and *toc1-2* (*53*), along with *gi-200* (*26*), *soc1-2* (*54*), *ft-10*, and *flc-1* (Arabidopsis Biological Resource Center) seeds were sown on 0.5× mass spectrometry (MS) agar and stratified for 3 days and then germinated in separate growth cabinets, each with a different light regime. After 4 days, seedlings were transplanted into pots filled with soil. Homozygous photoreceptor mutants *phyA*, *phyB*, *phyC*, *phyD*, *phyE*, *cry1*, *cry2*, and *cry1 cry2* plants (*55*) were stratified, germinated, and grown as described above. For imaging and flowering time experiments, one seedling was grown per pot (in 6.3-cm pots). For proteomics and RNA-seq, six seedlings were grown in larger 10-cm pots. All experiments (except where indicated) used a base 12-hour light/12-h dark photoperiod.

Imaging and computer vision analysis

Plants were imaged using Arducam 5MP OV5647 cameras (www.arducam.com/product/arducam-m12-night-vision-ir-cut-raspberry-pi-camera/), with images taken every 5 min between ZT0 and ZT12 for multiple days. Images were then processed using a customized version of PlantCV to identify individual plants from a whole tray image, measuring their total leaf area and perimeter. Briefly, one or more representative images from each growth chamber configure our PlantCV pipeline and output a configuration file that is used to bulk analyze images taken by the same camera for each experiment. These images are first undistorted using the camera intrinsic matrix and distortion coefficients obtained by calibrating cameras with the OpenCV fisheye camera model. The white balance of the images is then adjusted using a reference white spot fixed on our plant growth trays and the built-in PlantCV 'white_balance' function. Regions of interest (ROIs) around each individual plant are then manually drawn using a custom graphical user interface (GUI) ROI Drawing Tool that was based on a tool created by GitHub user BoKuan Liu (https://github.com/DennisLiu1993/Zoom-In-Out-with-OpenCV). Next, images are segmented into "plant" and "background" with a color threshold using a custom GUI-based HSV Thresholding Tool. After successful thresholding, optimized parameters are exported into a JSON configuration file. Subsequently, all images obtained from each camera for an experiment are analyzed using the configuration file produced for that camera. The image processing pipeline accepts the configuration file as input and produces two types of outputs. The first output is a comma-separated values (CSV) file for each camera, containing extracted plant traits along with metadata for each sample. The second output is the set of annotated images produced by PlantCV, which can be used to visually inspect the quality of the image analysis. Final plant area analysis across twilight lengths was performed by averaging the area of each plant measured during a 1-hour period (ZT 5.5 to 6.5) at 25 days after imbibition to avoid interference from leaf movement effects. Next, the averaged area at 25 days after imbibition per plant was plotted and a one-way ANOVA and Tukey's post hoc test with an adjusted *P* value threshold of 0.05 were applied to detect significant changes between twilight treatments. Final plant area measurements are provided in table S2. Raw and processed images can be downloaded from www.doi.org/10.5281/zenodo.7977125.

RNA-seq and transcriptome data analysis

Total RNA was extracted from rosette tissue harvested at ZT 23 on day 25 after imbibition ($n = 4$ biological replicates) using the Direct-zol-96 MagBead RNA kit (Zymo Research). RNA was checked for degradation using a TapeStation 4150 (Agilent) following the manufacturer's protocol. Cost-effective RNA-seq was performed using a miniaturized library preparation protocol by applying the Smart-seq2 single-cell method on bulk RNA. For this, cDNA was generated following the protocol as described in (*46*) with the following adjustment: 1 μl of lysate was transferred from the lysis plate into a new plate containing the RT mix. Preamplification of cDNA used 23 polymerase chain reaction cycles and was purified using Agencourt Ampure XP beads (Beckman Coulter) with a modified bead: DNA ratio of 0.8×. The quality of cDNA was checked using an NGS Fragment High Sensitivity Analysis Kit (Advanced Analytical) and a Fragment Analyzer (Advanced Analytical). The cDNA concentration was measured using a Qubit High-Sensitivity dsDNA Kit. Libraries were prepared using a Nextera XT DNA Library Preparation Kit (Illumina), using a standard protocol but with all reaction volumes reduced by 1/10 to accommodate the automation of the prep on the Echo LabCyte liquid handler (Beckman). Libraries were purified using Agencourt Ampure XP beads (Beckman Coulter). The size distribution of library pools was checked using a Fragment Analyzer and an NGS Fragment High Sensitivity Analysis Kit. Samples were pooled equimolar, and the final pool was quantified with the Kapa library quantification kit (Roche). The final pool was sequenced on a NovaSeq 6000 to produce paired-end 150–base pair reads, with an average read depth of 10 M reads per sample.

Protocol quality control of raw reads was performed with FastQC ver. 0.11.7 (*56*). Adapters were filtered with Trimmomatic v0.39 (*57*). Splice-aware alignment was performed with Star (*58*) against the Arabidopsis Araport 11 reference genome using the default parameters. Reads mapping to multiple loci in the reference genome were discarded. Quantification of reads per gene was performed with FeatureCounts from Subread package (*59*). Count-based differential expression analysis was done with the R-based Bioconductor package DESeq2 (*60*). Reported *P* values were adjusted for multiple testing by controlling the false discovery rate using the Benjamini-Hochberg procedure; Log_2 fold change > 0.58.

Proteomics sample preparation, mass spectrometry, and data analysis

Tissue extraction and sample processing

Frozen rosette tissue ($n = 4$ biological replicates) was ground using Geno/Grinder (SPEX SamplePrep) for 30 s at 1200 rpm and aliquoted into 100 mg fractions under liquid N_2 before extraction. Ground tissue was then dissolved in protein extraction buffer [50 mM Hepes-KOH (pH 8.0), 100 mM NaCl, and 4% (w/v) SDS at a 1:3 (w/v) ratio] and extracted by shaking 1000 RPM 95°C using a tabletop shaker (Eppendorf ThermoMixer F2.0). Samples were then centrifuged at 20,000*g* for 10 min at room temperature and the supernatant was retained in new tubes. Protein extracts were then reduced

with 10 mM dithiothreitol (D9779, Sigma-Aldrich) for 5 min at 95°C, followed by alkylation for 30 min with 55 mM iodoacetamide (I1149, Sigma-Aldrich) at room temperature. Total proteome peptide fractions were then generated using a Kingfisher Apex (Thermo Fisher Scientific) automated sample processing system as outlined by Leutert *et al.* (*61*) without deviation. Peptides were digested using sequencing grade trypsin (V5113, Promega) diluted in 50 mM triethylammonium bicarbonate buffer pH 8.5 (T7408, Sigma-Aldrich). Following digestion, samples were acidified with trifluoroacetic acid (A117, Thermo Fisher Scientific) to a final concentration of 0.5% (v/v). Peptides were desalted as previously described (*62*) using an OT-2 liquid handling robot (Opentrons Labworks Inc.) mounted with Omix C18 pipette tips (A5700310K, Agilent). Desalted peptides were dried and stored at −80°C before resuspension in 3.0% (v/v) acetonitrile (ACN)/0.1% (v/v) formic acid (FA) before MS injection.

LC-MS/MS analysis

Peptides were analyzed on a Fusion Lumos Orbitrap mass spectrometer (Thermo Fisher Scientific) in data-independent acquisition (DIA) mode. A total of 1 μg of the resuspended peptide was injected per replicate using an Easy-nLC 1200 system (LC140, Thermo Fisher Scientific) mounted with an Acclaim PepMap 100 C18 trap column (catalog no. 164750, Thermo Fisher Scientific) and a 50-cm Easy-Spray PepMap C18 analytical column (ES903, Thermo Fisher Scientific) warmed to 50°C. Peptides were eluted at 300 nl/min using a segmented solvent B gradient of 0.1% (v/v) FA in 80% (v/v) ACN (A998, Thermo Fisher Scientific) from 4 to 41% solvent B (0 to 120 min). A positive ion spray voltage of 2.3 kV was used with an ion transfer tube temperature of 300°C and an RF lens setting of 40%. BoxCar DIA acquisition was also performed as described (*45*) without any deviation. Briefly, MS1 spectra were acquired using two multiplexed targeted SIM scans of 10 BoxCar windows each. Full scan MS1 spectra [350 to 1400 mass/charge ratio (m/z)] were acquired with a resolution of 120,000 at 200 m/z and normalized AGC targets of 100% per BoxCar isolation window. Fragment spectra were acquired with a resolution of 30,000 across 28 38.5-m/z windows overlapping of 1 m/z using a dynamic maximum injection time and an AGC target value of 2000%, with a minimum number of desired points across each peak set to 6. HCD fragmentation was performed using a fixed 27% fragmentation energy.

Data analysis

Data were analyzed using Spectronaut ver. 17 (Biognosys AG), with all analysis details found in the Spectronaut result summary (table S2). Significantly changing differentially abundant proteins were determined and corrected for multiple comparisons (Bonferroni-corrected $P < 0.05$; q value; Log_2 fold change; $\text{Log}_2\text{FC} > 0.58$) (Fig. 4, A to D), while significantly changing proteins plotted across each time-point (Fig. 4E) were deduced using Perseus ver. 1.6.15.0 (*63*), with row valid values set to 100% and a Benjamini-Hochberg–corrected ANOVA $P < 0.05$.

Supplementary Materials

This PDF file includes:

Figs. S1 to S4

Legends for tables S1 to S9

Other Supplementary Material for this manuscript includes the following:

Tables S1 to S9

REFERENCES AND NOTES

1. N. Creux, S. Harmer, Circadian rhythms in plants. *Cold Spring Harb. Perspect. Biol.* **11**, a034611 (2019).
2. A. A. R. Webb, M. Seki, A. Satake, C. Caldana, Continuous dynamic adjustment of the plant circadian oscillator. *Nat. Commun.* **10**, 550 (2019).
3. R. A. Hut, S. Paolucci, R. Dor, C. P. Kyriacou, S. Daan, Latitudinal clines: An evolutionary view on biological rhythms. *Proc. Biol. Sci.* **280**, 20130433 (2013).
4. J. L. Weller, L. C. Liew, V. F. G. Hecht, V. Rajandran, R. E. Laurie, S. Ridge, B. Wenden, J. K. Vander Schoor, O. Jaminon, C. Blassiau, M. Dalmais, C. Rameau, A. Bendahmane, R. C. Macknight, I. Lejeune-Hénaut, A conserved molecular basis for photoperiod adaptation in two temperate legumes. *Proc. Natl. Acad. Sci. U.S.A.* **109**, 21158–21163 (2012).
5. S. Faure, A. S. Turner, D. Gruszka, V. Christodoulou, S. J. Davis, M. von Korff, D. A. Laurie, Mutation at the circadian clock gene EARLY MATURITY 8 adapts domesticated barley (Hordeum vulgare) to short growing seasons. *Proc. Natl. Acad. Sci. U.S.A.* **109**, 8328–8333 (2012).
6. C. R. McClung, Circadian clock components offer targets for crop domestication and improvement. *Genes* **12**, 374 (2021).
7. D. D. Seaton, A. Graf, K. Baerenfaller, M. Stitt, A. J. Millar, W. Gruissem, Photoperiodic control of the Arabidopsis proteome reveals a translational coincidence mechanism. *Mol. Syst. Biol.* **14**, e7962 (2018).
8. M. L. Sorkin, K. K. Markham, S. Zorich, A. Menon, K. N. Edgeworth, A. Ricono, D. Bryant, R. Bart, D. A. Nusinow, K. Greenham, Assembly and operation of an imaging system for long-term monitoring of bioluminescent and fluorescent reporters in plants. *Plant Methods* **19**, 19 (2023).
9. A. Flis, R. Sulpice, D. D. Seaton, A. A. Ivakov, M. Liput, C. Abel, A. J. Millar, M. Stitt, Photoperiod-dependent changes in the phase of core clock transcripts and global transcriptional outputs at dawn and dusk in Arabidopsis. *Plant Cell Environ.* **39**, 1955–1981 (2016).
10. M.-J. Park, Y.-J. Kwon, K.-E. Gil, C.-M. Park, LATE ELONGATED HYPOCOTYL regulates photoperiodic flowering via the circadian clock in *Arabidopsis*. *BMC Plant Biol.* **16**, 114 (2016).
11. M. T. Zagotta, K. A. Hicks, C. I. Jacobs, J. C. Young, R. P. Hangarter, D. R. Meeks-Wagner, The *Arabidopsis* ELF3 gene regulates vegetative photomorphogenesis and the photoperiodic induction of flowering. *Plant J.* **10**, 691–702 (1996).
12. S. Fowler, K. Lee, H. Onouchi, A. Samach, K. Richardson, B. Morris, G. Coupland, J. Putterill, GIGANTEA: A circadian clock-controlled gene that regulates photoperiodic flowering in Arabidopsis and encodes a protein with several possible membrane-spanning domains. *EMBO J.* **18**, 4679–4688 (1999).
13. M. T. Zagotta, S. Shannon, C. Jacobs, D. R. Meeks-Wagner, Early-flowering mutants of *Arabidopsis thaliana*. *Funct. Plant Biol.* **19**, 411–418 (1992).
14. NOAA National Centers for Environmental Information, "Monthly Global Climate Report for November 2023" (NOAA National Centers for Environmental Information, 2023); www.ncei.noaa.gov/access/monitoring/monthly-report/global/202311.
15. A. Ceglar, M. Zampieri, A. Toreti, F. Dentener, Observed northward migration of agro-climate zones in europe will further accelerate under climate change. *Earth's Future* **7**, 1088–1101 (2019).
16. L. L. Sloat, S. J. Davis, J. S. Gerber, F. C. Moore, D. K. Ray, P. C. West, N. D. Mueller, Climate adaptation by crop migration. *Nat. Commun.* **11**, 1243 (2020).
17. M. King, D. Altdorff, P. Li, L. Galagedara, J. Holden, A. Unc, Northward shift of the agricultural climate zone under 21st-century global climate change. *Sci. Rep.* **8**, 7904 (2018).
18. Y. H. Song, A. Kubota, M. S. Kwon, M. F. Covington, N. Lee, E. R. Taagen, D. Laboy Cintrón, D. Y. Hwang, R. Akiyama, S. K. Hodge, H. Huang, N. H. Nguyen, D. A. Nusinow, A. J. Millar, K. K. Shimizu, T. Imaizumi, Molecular basis of flowering under natural long-day conditions in Arabidopsis. *Nat. Plants.* **4**, 824–835 (2018).
19. N. Lee, Y. Ozaki, A. K. Hempton, H. Takagi, S. Purusuwashi, Y. H. Song, M. Endo, A. Kubota, T. Imaizumi, The FLOWERING LOCUS T gene expression is controlled by high-irradiance response and external coincidence mechanism in long days in Arabidopsis. *New Phytol.* **239**, 208–221 (2023).
20. M. A. Gehan, N. Fahlgren, A. Abbasi, J. C. Berry, S. T. Callen, L. Chavez, A. N. Doust, M. J. Feldman, K. B. Gilbert, J. G. Hodge, J. S. Hoyer, A. Lin, S. Liu, C. Lizárraga, A. Lorence, M. Miller, E. Platon, M. Tessman, T. Sax, PlantCV v2: Image analysis software for high-throughput plant phenotyping. *PeerJ.* **5**, e4088 (2017).
21. N. Fahlgren, M. Feldman, M. A. Gehan, M. S. Wilson, C. Shyu, D. W. Bryant, S. T. Hill, C. J. McEntee, S. N. Warnasooriya, I. Kumar, T. Ficor, S. Turnipseed, K. B. Gilbert, T. P. Brutnell, J. C. Carrington, T. C. Mockler, I. Baxter, A versatile phenotyping system and analytics platform reveals diverse temporal responses to water availability in setaria. *Mol. Plant* **8**, 1520–1535 (2015).
22. S. Pouteau, C. Albertini, The significance of bolting and floral transitions as indicators of reproductive phase change in Arabidopsis. *J. Exp. Bot.* **60**, 3367–3377 (2009).
23. J. T. Anderson, C.-R. Lee, T. Mitchell-Olds, Life-history QTLS and natural selection on flowering time in Boechera stricta, a perennial relative of Arabidopsis. *Evolution* **65**, 771–787 (2011).

24. E. J. Austen, A. E. Weis, What drives selection on flowering time? An experimental manipulation of the inherent correlation between genotype and environment. *Evolution* **69**, 2018–2033 (2015).
25. J. Friedman, A. D. Twyford, J. H. Willis, B. K. Blackman, The extent and genetic basis of phenotypic divergence in life history traits in Mimulus guttatus. *Mol. Ecol.* **24**, 111–122 (2015).
26. R. I. Colautti, J. Ågren, J. T. Anderson, Phenological shifts of native and invasive species under climate change: Insights from the Boechera-Lythrum model. *Philos. Trans. R. Soc. Lond. B Biol. Sci.* **372**, 20160032 (2017).
27. S. Pouteau, V. Ferret, D. Lefebvre, Comparison of environmental and mutational variation in flowering time in Arabidopsis. *J. Exp. Bot.* **57**, 4099–4109 (2006).
28. Q. Wang, W. Liu, C. C. Leung, D. A. Tart, J. M. Gendron, Parallel mechanisms detect different photoperiods to independently control seasonal flowering and growth in plants. bioRxiv 2023.02.10.528016 (2023).
29. T. A. Moraes, V. Mengin, M. G. Annunziata, B. Encke, N. Krohn, M. Höhne, M. Stitt, Response of the circadian clock and diel starch turnover to one day of low light or low CO_2. *Plant Physiol.* **179**, 1457–1478 (2019).
30. G. Marino, M. Aqil, B. Shipley, The leaf economics spectrum and the prediction of photosynthetic light-response curves. *Funct. Ecol.* **24**, 263–272 (2010).
31. H. Guo, H. Yang, T. C. Mockler, C. Lin, Regulation of flowering time by *Arabidopsis* photoreceptors. *Science* **279**, 1360–1363 (1998).
32. K. J. Halliday, M. Koornneef, G. C. Whitelam, Phytochrome B and at least one other phytochrome mediate the accelerated flowering response of Arabidopsis thaliana L. to low red/far-red ratio. *Plant Physiol.* **104**, 1311–1315 (1994).
33. K. J. Halliday, G. C. Whitelam, Changes in photoperiod or temperature alter the functional relationships between phytochromes and reveal roles for phyD and phyE. *Plant Physiol.* **131**, 1913–1920 (2003).
34. P. F. Devlin, P. R. Robson, S. R. Patel, L. Goosey, R. A. Sharrock, G. C. Whitelam, Phytochrome D acts in the shade-avoidance syndrome in Arabidopsis by controlling elongation growth and flowering time. *Plant Physiol.* **119**, 909–915 (1999).
35. Y. Niwa, S. Ito, N. Nakamichi, T. Mizoguchi, K. Niinuma, T. Yamashino, T. Mizuno, Genetic linkages of the circadian clock-associated genes, TOC1, CCA1 and LHY, in the photoperiodic control of flowering time in Arabidopsis thaliana. *Plant Cell Physiol.* **48**, 925–937 (2007).
36. P. F. Devlin, S. A. Kay, Cryptochromes are required for phytochrome signaling to the circadian clock but not for rhythmicity. *Plant Cell* **12**, 2499–2509 (2000).
37. X. Wang, B. Jiang, L. Gu, Y. Chen, M. Mora, M. Zhu, E. Noory, Q. Wang, C. Lin, A photoregulatory mechanism of the circadian clock in Arabidopsis. *Nat. Plants.* **7**, 1397–1408 (2021).
38. W. Mo, J. Zhang, L. Zhang, Z. Yang, L. Yang, N. Yao, Y. Xiao, T. Li, Y. Li, G. Zhang, M. Bian, X. Du, Z. Zuo, Arabidopsis cryptochrome 2 forms photobodies with TCP22 under blue light and regulates the circadian clock. *Nat. Commun.* **13**, 2631 (2022).
39. S. E. Sanchez, M. L. Rugnone, S. A. Kay, Light perception: A matter of time. *Mol. Plant* **13**, 363–385 (2020).
40. D. H. Park, D. E. Somers, Y. S. Kim, Y. H. Choy, H. K. Lim, M. S. Soh, H. J. Kim, S. A. Kay, H. G. Nam, Control of circadian rhythms and photoperiodic flowering by the Arabidopsis GIGANTEA gene. *Science* **285**, 1579–1582 (1999).
41. Y.-J. Park, J. Y. Kim, J.-H. Lee, B.-D. Lee, N.-C. Paek, C.-M. Park, GIGANTEA shapes the photoperiodic rhythms of thermomorphogenic growth in arabidopsis. *Mol. Plant* **13**, 459–470 (2020).
42. Z. Wu, X. Fang, D. Zhu, C. Dean, Autonomous pathway: *FLOWERING LOCUS C* repression through an antisense-mediated chromatin-silencing mechanism. *Plant Physiol.* **182**, 27–37 (2020).
43. M. Johansson, D. Staiger, Time to flower: Interplay between photoperiod and the circadian clock. *J. Exp. Bot.* **66**, 719–730 (2015).
44. R. G. H. Immink, D. Posé, S. Ferrario, F. Ott, K. Kaufmann, F. L. Valentim, S. de Folter, F. van der Wal, A. D. J. van Dijk, M. Schmid, G. C. Angenent, Characterization of SOC1's central role in flowering by the identification of its upstream and downstream regulators. *Plant Physiol.* **160**, 433–449 (2012).
45. D. Mehta, S. Scandola, R. G. Uhrig, BoxCar and library-free data-independent acquisition substantially improve the depth, range, and completeness of label-free quantitative proteomics. *Anal. Chem.* **94**, 793–802 (2022).
46. S. Picelli, O. R. Faridani, A. K. Björklund, G. Winberg, S. Sagasser, R. Sandberg, Full-length RNA-seq from single cells using Smart-seq2. *Nat. Protoc.* **9**, 171–181 (2014).
47. D. Szklarczyk, A. L. Gable, D. Lyon, A. Junge, S. Wyder, J. Huerta-Cepas, M. Simonovic, N. T. Doncheva, J. H. Morris, P. Bork, L. J. Jensen, C. von Mering, STRING v11: Protein-protein association networks with increased coverage, supporting functional discovery in genome-wide experimental datasets. *Nucleic Acids Res.* **47**, D607–D613 (2019).
48. M. W. Oravec, K. Greenham, The adaptive nature of the plant circadian clock in natural environments. *Plant Physiol.* **190**, 968–980 (2022).
49. E. J. Blair, T. Bonnot, M. Hummel, E. Hay, J. M. Marzolino, I. A. Quijada, D. H. Nagel, Contribution of time of day and the circadian clock to the heat stress responsive transcriptome in Arabidopsis. *Sci. Rep.* **9**, 4814 (2019).
50. P. Y. Hsu, U. K. Devisetty, S. L. Harmer, Accurate timekeeping is controlled by a cycling activator in Arabidopsis. *eLife* **2**, e00473 (2013).
51. J.-H. Jung, A. D. Barbosa, S. Hutin, J. R. Kumita, M. Gao, D. Derwort, C. S. Silva, X. Lai, E. Pierre, F. Geng, S.-B. Kim, S. Baek, C. Zubieta, K. E. Jaeger, P. A. Wigge, A prion-like domain in ELF3 functions as a thermosensor in Arabidopsis. *Nature* **585**, 256–260 (2020).
52. D. A. Nusinow, A. Helfer, E. E. Hamilton, J. J. King, T. Imaizumi, T. F. Schultz, E. M. Farré, S. A. Kay, The ELF4-ELF3-LUX complex links the circadian clock to diurnal control of hypocotyl growth. *Nature* **475**, 398–402 (2011).
53. C. Strayer, T. Oyama, T. F. Schultz, R. Raman, D. E. Somers, P. Más, S. Panda, J. A. Kreps, S. A. Kay, Cloning of the Arabidopsis clock gene TOC1, an autoregulatory response regulator homolog. *Science* **289**, 768–771 (2000).
54. D. C. Wilson, P. Carella, M. Isaacs, R. K. Cameron, The floral transition is not the developmental switch that confers competence for the Arabidopsis age-related resistance response to Pseudomonas syringae pv. tomato. *Plant Mol. Biol.* **83**, 235–246 (2013).
55. I. Sherr, "Regulation of auxin transport in Arabidopsis leaf vascular development," thesis, University of Alberta, Edmonton, AB (2012); doi:10.7939/r38x2d.
56. S. Andrews, *FastQC A Quality Control tool for High Throughput Sequence Data* (Babraham Bioinformatics, 2010); www.bioinformatics.babraham.ac.uk/projects/fastqc/.
57. A. M. Bolger, M. Lohse, B. Usadel, Trimmomatic: A flexible trimmer for Illumina sequence data. *Bioinformatics* **30**, 2114–2120 (2014).
58. A. Dobin, C. A. Davis, F. Schlesinger, J. Drenkow, C. Zaleski, S. Jha, P. Batut, M. Chaisson, T. R. Gingeras, STAR: Ultrafast universal RNA-seq aligner. *Bioinformatics* **29**, 15–21 (2013).
59. Y. Liao, G. K. Smyth, W. Shi, The Subread aligner: Fast, accurate and scalable read mapping by seed-and-vote. *Nucleic Acids Res.* **41**, e108 (2013).
60. M. I. Love, W. Huber, S. Anders, Moderated estimation of fold change and dispersion for RNA-seq data with DESeq2. *Genome Biol.* **15**, 550 (2014).
61. M. Leutert, R. A. Rodríguez-Mias, N. K. Fukuda, J. Villén, R2-P2 rapid-robotic phosphoproteomics enables multidimensional cell signaling studies. *Mol. Syst. Biol.* **15**, e9021 (2019).
62. R. G. Uhrig, P. Schläpfer, B. Roschitzki, M. Hirsch-Hoffmann, W. Gruissem, Diurnal changes in concerted plant protein phosphorylation and acetylation in Arabidopsis organs and seedlings. *Plant J.* **99**, 176–194 (2019).
63. S. Tyanova, T. Temu, P. Sinitcyn, A. Carlson, M. Y. Hein, T. Geiger, M. Mann, J. Cox, The Perseus computational platform for comprehensive analysis of (prote)omics data. *Nat. Methods* **13**, 731–740 (2016).

Acknowledgments: We would like to thank J. Pruneda-Paz (University of California, San Diego) for providing *lhy-20 cca1-1* seeds and S. Harmer (University of California, Davis) for providing *rve 4-1 6-1 8-1* and *toc1-2* seeds. We acknowledge G2V Optics Inc. for lighting equipment and support, J. Moore from the Alberta Proteomics and Mass Spectrometry Facility, and A. Verfaillie, K. Mirzai, and A. C. Calabuig from the GenomicsCore Leuven for technical support. **Funding:** Funding for this research was provided by the National Science and Engineering Research Council of Canada (NSERC), Alberta Innovates (AI), MITACs, the Canada Foundation for Innovation (CFI), and the Bijzonder Onderzoeksfonds start-up grant (#3E221118) by KU Leuven. D.M. was supported by a Swiss National Science Foundation Early Postdoc Mobility grant (#181602) for a part of the duration of the project. **Author contributions:** Conceptualization: D.M. and R.G.U. Investigation: D.M., S.S., M.C.R.G., L.E.G., and C.L. Formal Analysis: D.M., M.T., E.S., and R.G.U. Methodology: D.M., S.S., and R.G.U. Data curation: D.M., S.S., C.K., and R.G.U. Writing—original draft: D.M. and R.G.U. Visualization: D.M. Writing—review and editing: D.M., R.G.U., S.S., M.T., C.K., and E.S. Software: C.K. Supervision: R.G.U. Project administration: R.G.U. Funding acquisition: R.G.U. and D.M. **Competing interests:** The authors declare that they have no competing interests. **Data and materials availability:** All raw proteomics data can be found through the PRoteomics IDEntifications Database (PRIDE) using the dataset identifier PXD039428. All raw image data can be found on Zenodo (www.doi.org/10.5281/zenodo.7977125). RNA sequencing data have been deposited in the European Nucleotide Archive (ENA) at EMBL-EBI under accession number PRJEB62130. The code used to analyze image data, perform *k*-means clustering, and plot graphs is available on Zenodo at https://zenodo.org/doi/10.5281/zenodo.11099747 and on GitHub at https://github.com/UhrigLab/twilight_length. All data needed to evaluate the conclusions in the paper are present in the paper and/or the Supplementary Materials.

Submitted 11 October 2023
Accepted 28 May 2024
Published 28 June 2024
10.1126/sciadv.adl3199